Int J Thermophys (2013) 34:1429–1434
DOI 10.1007/s10765-013-1441-z

Equivalence of Normalized Thermal-Wave Fields Between Curved and Flat Surfaces and Its Application in the Characterization of Curved Samples

Chinhua Wang · Jie Zhang · Liwang Liu · Andreas Mandelis

Received: 13 February 2012 / Accepted: 5 April 2013 / Published online: 1 May 2013

Abstract Equivalence of the normalized thermal-wave fields between curved and flat surfaces under certain conditions is investigated based on theoretical models of cylindrical, spherical, and flat solids with multilayer structures. The principle and the physical mechanism of the elimination of the surface curvature effect from the overall photothermal signal of the curvilinear solid are suggested. The effects of the relative values of radii of curvature of the curvilinear solid, the thickness of the inhomogeneous surface layer, and the measurement azimuthal angle on the validity of the equivalence principle are discussed. Consistent experimental reconstructions of thermophysical depth profiles of hardened cylindrical steel rods of various diameters are performed and obtained based on both the curvilinear theory and the equivalent flat surface theory.

Keywords Curvilinear surface · Equivalence · Flat surface · Normalized thermal-wave fields

1 Introduction

Laser-induced photothermal radiometry (PTR) is a powerful tool for the thermophysical characterization of broad classes of materials [1] since the late 1980s. With the increasing applications of PTR to materials characterization, recent studies have been

C. Wang (✉) · J. Zhang · L. Liu
Institute of Modern Optical Technologies, Soochow University,
Suzhou 215006, Jiangsu, China
e-mail: chinhua.wang@suda.edu.cn

A. Mandelis
Center for Advanced Diffusion-Wave Technologies (CADIFT),
Department of Mechanical and Industrial Engineering, University of Toronto,
Toronto, ON M5S 3G8, Canada

extended to the evaluation of curvilinear samples. Mathematical models of cylindrical and spherical samples have been developed using the Green function method and the quadrupole method [2–7] for both homogeneous and multilayer structures. These results established theoretical bases for characterizing cylindrical and spherical solids, if all the geometrical and measurement parameters are precisely known. Recently, Liu et al. [8,9] reported that the effect of the radius of curvature of cylindrical solids can be eliminated or suppressed using a similarity normalization (SN) method. The mechanism was explained using a simplified two-layer theoretical model or quadruple method [4]. In this article, we present an investigation (both spherical and cylindrical solids) of the methodology based on multilayer models using the Green function method.

2 Theory

A case hardened steel (with a flat, cylindrical, spherical, or other curvilinear surface) may be a typical inhomogeneous structure with an outer hardened layer in which the radial thermophysical property (e.g., thermal conductivity and/or hardness) varies continuously down to a homogeneous unhardened inner layer. To characterize these types of solids, multilayer theoretical models must be developed and employed for each type of curvature. Figure 1 shows the geometries and the coordinates of multilayer cylindrical (Fig. 1a), spherical (Fig. 1b), and flat (Fig. 1c) structures. All three types of solids are assumed to consist of N layers. The thermophysical properties of the ith layer are labelled (k_i, α_i), where k_i and α_i are the thermal conductivity and thermal diffusivity, respectively. The curvilinear solids are illuminated with a uniform light beam impinging on part of their surface subtending a sector of angle θ_0 for a cylinder and 2Ψ for a sphere (shown in Fig. 1a and b). The incident beam is intensity modulated at frequency f. The thermal-wave fields of a multilayered cylindrical and spherical solid sample with outer radius r_N and inner radii $r_{N-1}, r_{N-2}, \ldots, r_1 (b = r_N > r_{N-1} > r_{N-2} > \cdots > r_1 = a)$ can be derived by the Green's function method. For cylindrical and flat solids, the thermal-wave fields in the outmost region can be found in Refs. [6] and [10], respectively. For spherical samples, the thermal-wave field is given by [7]

$$T(\vec{r}, \omega) = \frac{F_0}{4k_n} \left\{ g^N(r_1, r_2, \ldots r_N, r)|_{l=0} \frac{\sin^2 \psi}{2} + g^N(r_1, r_2, \ldots r_N, r)|_{l=1} \times \cos\theta (1 - \cos^3 \psi) - \sum_{l=2}^{\infty} g^N(r_1, r_2, \ldots r_N, r) \frac{(2l+1)\sin\psi}{(l-1)(l+2)} \times P_l(\cos\theta)[\sin\psi P_l(\cos\psi) + \cos\psi P_l^1(\cos\psi)] \right\}, \quad (1)$$

where $\kappa_N \equiv \mathrm{i}\sigma_N = -(1-\mathrm{i})\sqrt{\omega/2\alpha_N}$, and

$$g^N(r_1, r_2, \ldots r_N, r) = \frac{j_l(\kappa_N r) X_{N\cdots 321} - n_l(\kappa_N r) Y_{N\cdots 321}}{j_l'(\kappa_N r_N) X_{N\cdots 321} - n_l'(\kappa_N r_N) Y_{N\cdots 321}},$$

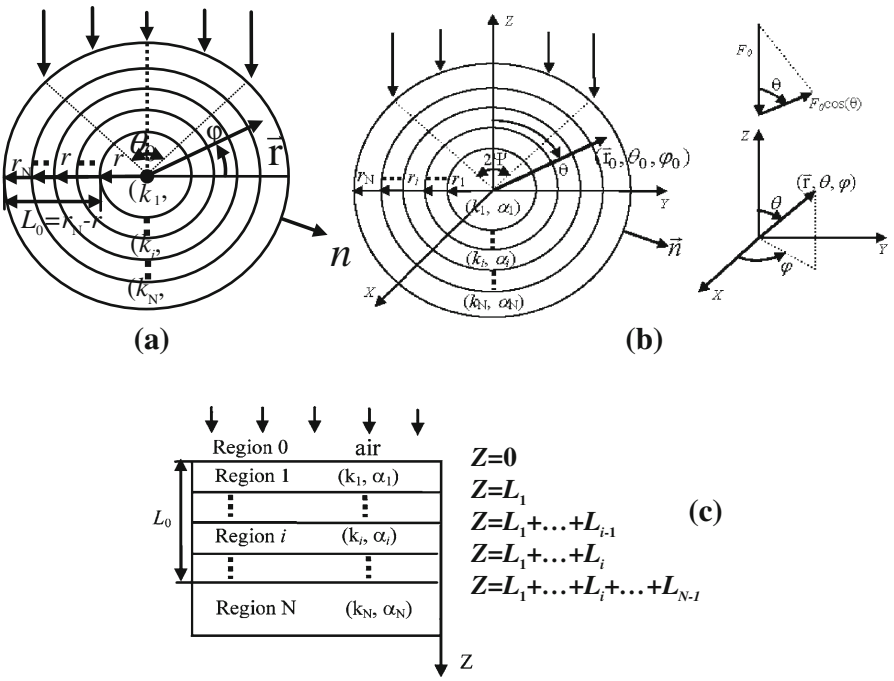

Fig. 1 Geometry and coordinates of multilayer (a) cylinder, (b) sphere, and (c) flat structures. All three samples are assumed to consist of N layers each

with

$$\begin{bmatrix} X_{N\cdots 321} \\ Y_{N\cdots 321} \end{bmatrix} = \begin{bmatrix} \beta_{N,N-1} n_l'(\kappa_N r_{N-1}), & -n_l(\kappa_N r_{N-1}) \\ \beta_{N,N-1} j_l'(\kappa_N r_{N-1}), & -j_l(\kappa_N r_{N-1}) \end{bmatrix} \begin{bmatrix} j_l(\kappa_{N-1} r_{N-1}), & -n_l(\kappa_{N-1} r_{N-1}) \\ j_l'(\kappa_{N-1} r_{N-1}), & -n_l'(\kappa_{N-1} r_{N-1}) \end{bmatrix} \begin{bmatrix} X_{N-1\cdots 21} \\ Y_{N-1\cdots 21} \end{bmatrix}, \tag{2}$$

and $\beta_{N,N-1} = k_N/k_{N-1}$. j_l, n_l, j_l', n_l' are the complex-argument spherical Bessel functions of order l of the first and second kinds, and their derivative, respectively. $P_l(\cos\theta)$ is a Legendre polynomial.

3 Numerical Calculation

We first assume a mathematical description of the inhomogeneous thermal conductivity/diffusivity depth profile in which the thermal parameter is a monotonic function of depth, r, and saturates at a pre-determined depth to conform with the unhardened bulk of the sample [9,10]:

$$k(r) = k_0 \left(\frac{1 + \Delta \mathrm{e}^{-Qr}}{1 + \Delta} \right)^2, \text{ with } \Delta = \frac{1 - \sqrt{k'/k_0}}{\sqrt{k'/k_0} - \mathrm{e}^{-QL_0}}, \tag{3}$$

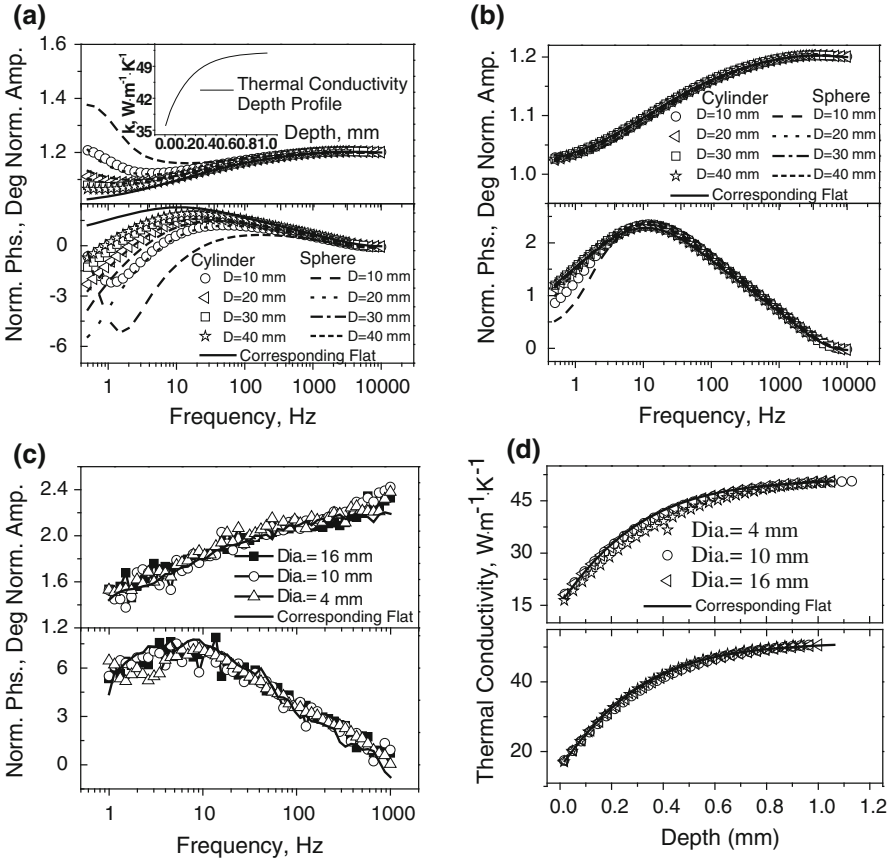

Fig. 2 (a) Amplitude and phase of thermal-wave field of the flat, cylindrical, and spherical solids with various radii of curvature. *Inset* Thermal-conductivity depth profile of the common inhomogeneous surface layer. (b) Normalized amplitude and phase of thermal-wave fields of cylindrical and spherical samples with different radii of curvature and that of the corresponding flat sample. (c) Experimental results of cylindrical rods with diameters of 4 mm, 10 mm, 16 mm, and the flat sample. (d) Comparison of the recovered thermal-conductivity depth profile based on the cylindrical theoretical model (*upper*) and the flat theoretical model (*lower*)

where k_0 and k' represent the thermal conductivity of the outermost and innermost layers, respectively, L_0 is the total thickness of the inhomogeneous surface layer (i.e., $r_N - r_1$), and the exponent Q represents the thermal gradient coefficient (mm^{-1}). Figure 2a shows the radius-of-curvature effect for various cylindrical and spherical samples on the thermal-wave signal frequency dependence and the comparison with that from the flat solid, where all the solids are assumed to have the same thermal-conductivity depth profile (shown in the inset). The depth profile was assumed with values $k_0 = 36.05\,\mathrm{W \cdot m^{-1} \cdot K^{-1}}$, $\alpha_0 = 9.43 \times 10^{-6}\,\mathrm{m^2 \cdot s^{-1}}$ at the surface, and $k' = 51.9\,\mathrm{W \cdot m^{-1} \cdot K^{-1}}$, $\alpha' = 13.57 \times 10^{-6}\,\mathrm{m^2 \cdot s^{-1}}$ at depth L_0 (AISI1018 steel is assumed [11]). The thickness of the inhomogeneous layer L_0 is assumed to be 1 mm. The exponent Q is $4500\,\mathrm{mm}^{-1}$. In Fig. 2a, the amplitudes and phases are normalized

by those of a semi-infinite flat homogeneous AISI1018 steel sample [12]. Cylinders and spheres with diameters $D = 10$ mm, 20 mm, 30 mm, and 40 mm and the corresponding inhomogeneous flat solids were investigated. The azimuthal angle φ was fixed at 90° and 0° for cylinders and spheres, respectively, Fig. 1. The incident beam subtends an angle of 180°. Figure 2a clearly shows the sensitivity of the thermal-wave signals on the radii of curvature of the solids. Figure 2b shows the results of curvature elimination based on the homogeneous and multilayer cylindrical and spherical models. Parameters (depth profile of thermal conductivity, radius of curvature, azimuthal angle) of the sample were exactly the same as those in Fig. 2a. The normalization was performed using a multilayered solid (cylinder or sphere) normalization with respect to the corresponding homogeneous counterparts with the same outer diameter. The thermophysical parameters of these homogeneous solids as well as those of the central region of the inhomogeneous solids were assumed to be unhardened AISI1018 steel. It is seen in Fig. 2b that the normalized amplitudes of solids with different diameters, including the flat solid, essentially coincide in the entire frequency range, which indicates that radius-of-curvature effects can be eliminated from the photothermal signal using the aforementioned normalization process. It should be noted that a residual memory of the curvature effect can be seen in the phase channel of Fig. 2b and c especially for small radii of the curvature in the low frequency range of <5 Hz. The significance of curvature elimination is that the curvilinear solid can be characterized using the current simple techniques existing for flat solids.

Experiments were performed to demonstrate the equivalence of the normalized thermal-wave signals between the flat surface and the curvilinear surfaces. Two sets of cylindrical AISI 1020 steel samples were machined with diameters of 4 mm, 10 mm, and 16 mm. One set of samples underwent a case hardening (carburizing) process as a batch, to ensure the same case depth profile, while the other set of samples was kept unhardened (reference). The thermophysical properties of AISI 1020 steel used in the depth profile reconstructions were: $k' = 50.63\,\mathrm{W \cdot m^{-1} \cdot K^{-1}}$, $\alpha' = 13.77 \times 10^{-6}\,\mathrm{m^2 \cdot s^{-1}}$. The experimental measurements were performed at the north-pole point of the curved surface of the cylindrical rods, i.e., 90° azimuthal angle was adopted. The PTR signal of flat solids was obtained by measuring the bottom (flat) surface of a 16 mm diameter cylindrical sample. It is seen from Fig. 2c that normalized amplitudes and phases obtained from curvilinear samples with various diameters overlap with the corresponding flat solid, albeit with some discrepancies at the low frequency range, especially for small diameters.

The experimental data were fitted using two different theoretical models and the reconstructed depth profiles of the thermal conductivity are shown in Fig. 2d. The detailed best-fit parameters are: $L_0 = 0.95$ mm, 0.98 mm, 1.02 mm, and 1.08 mm; $Q = 4805\,\mathrm{mm^{-1}}$, $3475\,\mathrm{mm^{-1}}$, $3666\,\mathrm{mm^{-1}}$, and $3975\ \mathrm{mm^{-1}}$; and $k_1 = 15.6\,\mathrm{W \cdot m^{-1} \cdot K^{-1}}$, $15.9\,\mathrm{W \cdot m^{-1} \cdot K^{-1}}$, $15.8\,\mathrm{W \cdot m^{-1} \cdot K^{-1}}$, and $15.3\,\mathrm{W \cdot m^{-1} \cdot K^{-1}}$ for cylinders with diameters of 4 mm, 10 mm, 16 mm, and flat sample, respectively, using the rectilinear model, and $L_0 = 1.05$ mm, 1.15 mm, and 1.07 mm, $\mathrm{Q} = 3100\,\mathrm{mm^{-1}}$, $3160\,\mathrm{mm^{-1}}$, and $3580\,\mathrm{mm^{-1}}$ using the cylindrical model for cylinders with diameters of 4 mm, 10 mm, and 16 mm, respectively. It is seen that the reconstructed depth profiles of the thermal conductivity with various diameters all approximately coincide with that of the flat solid no matter which theoretical model is used for reconstruction. This is consistent

with the theoretical demonstration and indicates that a curvilinear cylindrical depth profile can be characterized using the algorithm for a flat solid.

4 Conclusions

In summary, we have demonstrated that curvilinear solids can be characterized using a rectilinear theoretical model for flat solids on the basis of the SN. This is significant in that it enables the application of photothermal depth profilometric techniques, and PTR in particular, to inhomogeneous solids of cylindrical and spherical geometry.

Acknowledgments This study has been sponsored by the National Natural Science Foundation of China (Grant No. 60877063), Scientific Research Foundation for the Returned Overseas Chinese Scholars, Education Ministry of China, and the project of the Priority Academic Program Development (PAPD) of Jiangsu Higher Education Institutions. One of us (AM) is grateful to the Canada Foundation for Innovation (CFI) and the Ontario Research Fund (ORF) for instrumentation support.

References

1. D.P. Almond, P.M. Patel, *Photothermal Science and Techniques* (Chapman and Hall, London, 1996)
2. C. Wang, A. Mandelis, Y. Liu, J. Appl. Phys. **96**, 3756 (2004)
3. C. Wang, Y. Liu, A. Mandelis, J. Sun, J. Appl. Phys. **101**, 083503 (2007)
4. A. Salazar, R. Celorrio, J. Appl. Phys. **100**, 113535 (2006)
5. N. Madariaga, A. Salazar, J. Appl. Phys. **101**, 103534 (2007)
6. G. Xie, J. Zhang, L. Liu, C. Wang, A. Mandelis, J. Appl. Phys. **109**, 113534 (2011)
7. L. Liu, G. Xie, C. Wang, Proc. SPIE **7656**, 76563M (2010)
8. L. Liu, C. Wang, X. Yuan, A. Mandelis, J. Appl. Phys. **107**, 053503 (2010)
9. L. Liu, C. Wang, X. Yuan, A. Mandelis, J. Phys. D Appl. Phys. **43**, 285403 (2010)
10. Q. Hong, C. Wang, X. Guo, A. Mandelis, J. Appl. Phys. **104**, 113518 (2008)
11. R. Steiner, *Metals Handbook*, vol. 1, 10th edn. (ASM International, Materials Park, OH, 1990), p. 196
12. A. Mandelis, *Diffusion-Wave Fields: Mathematical Methods and Green Functions* (Springer, New York, 2001)